Gamma-ray spectral energy resolution calibration based on locally constrained regularization for scintillation detector response: methodology, numerical and experimental analysis*

Guo-Feng Yang,[1,2,†] Wen-Zheng Peng,[1] Dong-Ming Liu,[3] Xiao-Long Wu,[4] Meng Chen,[1] and Xiang-Jun Liu[1,2]

[1]*School of Geoscience and Technology, Southwest Petroleum University, Chengdu, 610500, Sichuan, China*
[2]*State Key Laboratory of Oil and Gas Reservoir Geology and Exploitation, Southwest Petroleum University, Chengdu, 610500, Sichuan, China*
[3]*China National Logging Corporation, Xian, 710200, Shanxi, China*
[4]*China Oilfield Services Limited, Langfang, 065201, Hebei, China*

Energy resolution calibration is crucial for gamma-ray spectral analysis, as measured using a scintillation detector. A locally constrained regularization method was proposed to determine the resolution calibration parameters. First, a Monte Carlo simulation model consistent with an actual measurement system was constructed to obtain the energy deposition distribution in the scintillation crystal. Subsequently, the regularization objective function is established based on weighted least squares and additional constraints. Additional constraints were designed using a special weighting scheme based on the incident gamma-ray energies. Subsequently, an intelligent algorithm was introduced to search for the optimal resolution calibration parameters by minimizing the objective function. The most appropriate regularization parameter was determined through mathematical experiments. When the regularization parameter was 30, the calibrated results exhibited the minimum RMSE. Simulations and test-pit experiments were conducted to verify the performance of the proposed method. The simulation results demonstrate that the proposed algorithm can determine resolution calibration parameters more accurately than the traditional weighted least squares, and the test pit experimental results show that the R-squares between the calibrated and measured spectra are larger than 0.99. The accurate resolution calibration parameters determined by the proposed method lay the foundation for gamma-ray spectral processing and simulation benchmarking.

Keywords: Energy resolution, Regularization, Gaussian broadening, Spectral analysis, Scintillation detector

I. INTRODUCTION

Gamma-rays are widely used in material detection, geological exploration, environmental monitoring, and other fields [1–8]. Recently, scintillation detectors have become one of the most popular devices for gamma-ray measurements owing to their many advantages in detection efficiency, power consumption, cost, and applicability [9, 10]. Scintillation crystals, such as Sodium Iodide (NaI), Gadolinium Orthosilicate (GSO), Bismuth Germanate (BGO), Gadolinium Yttrium Orthosilicate (GYSO), and Lanthanum Bromide ($LaBr_3$), have good stopping powers because of their high density and atomic number, making them suitable for radiation detection [11–14]. However, although incident gamma rays generally have definite energies, the gamma spectrum of the scintillation detector response is not an impulse signal. Factors such as the non-uniform luminous efficiency of the scintillation crystals and the statistical fluctuation of charge generated by ionization inside the detector can result in a peak shape at the intrinsic gamma-ray energy, which can be well approximated by a Gaussian function [15]. This type of Gaussian broadening can describe the scintillation detector response, particularly the energy resolution, which is characterized by the full width at half maximum (FWHM) quantity [16]. In qualitative and quantitative spectral analyses, energy resolution is a crucial parameter for evaluating the performance of a scintillation detector, which represents the ability of the detector to distinguish two close energies [17]. Moreover, to decompose the gamma spectrum and extract complicated component information from the spectrum, energy resolution calibration is essential for radiation measurement systems [18, 19]. In addition, in many gamma-ray spectroscopy applications, the spectral characteristic peaks may be well separated, weakly overlapping, or strongly overlapping, which is limited by the energy resolution. Accurate energy-resolution calibration is important for resolution enhancement, rapid component identification, spectral deconvolution, and other conventional spectral processes [20–23].

A standard method for calibrating the spectral energy resolution of a scintillation detector is to fit the peak shapes of different characteristic peaks using a Gaussian function. In general, with an increase in gamma ray energy, the width of the characteristic peak also increases, which is related to the scintillation crystal properties and conforms to a definite model. Therefore, the nonlinear parameters of the FWHM calibration curve can be calculated by using several characteristic peak widths [24]. The most common method for fitting a peak shape is the nonlinear iterative method [25, 26]. However, the main difficulty of this method is that it easily converges to a locally optimum solution in multidimensional cases, especially if a bad initial starting guess is given [27, 28]. In addition, sometimes poor energy resolution and Compton scattering result in a high background in the low-energy region of the measured spectrum, and some weak peaks are submerged in the background whose shapes are difficult to fit accurately. In this case, additional background correction processing is

* This work was supported by the National Natural Science Foundation of China (No.41804141), and the author thanks the support of the State Key Laboratory of Oil and Gas Reservoir Geology and Exploitation, Southwest Petroleum University, Sichuan Province, China.
† Corresponding author, guofeng_yang@swpu.edu.cn

necessary to obtain a pure peak, such as the SNIP method or the asymmetrical least squares method [29–31].

With the development of numerical simulation technology, the Monte Carlo method has played an increasingly important role in gamma-ray calibration [32, 33]. By establishing a simulation model consistent with the measurement system, the optimal nonlinear resolution calibration parameters can be obtained using an optimization method to minimize the error between the simulated and measured spectra [34]. However, in the absence of effective constraints, traditional optimization methods can easily induce unreasonable solutions, even if the adaptability of the objective function is satisfactory. Although the optimization performance can be improved by multiple restarts or increasing the number of iterations, this simultaneously reduces the efficiency of the optimization.

This study proposes a novel gamma spectral energy resolution calibration method based on the regularization theory. A Monte Carlo simulation was adopted to acquire the gamma-ray energy distribution in the scintillation detector. The intrinsic energies were then used as prior knowledge to set the constraints of the regularization equation. Subsequently, an intelligent optimization algorithm was introduced to solve the regularization equation, which was regarded as the objective function, realizing energy resolution matching between the calibrated and actual spectra. Thus, the optimal resolution calibration parameters were determined.

This paper is organized as follows: The theory of scintillation detector response and the concept of the proposed locally constrained regularization method are elaborated in the II section. In the III section, the simulation gamma-ray spectra, and test pit experimental spectra are used to verify the proposed method. The results of the spectral-resolution calibration were compared with those of the actual spectra, and the processing performance was discussed. Finally, the conclusions and suggestions are provided in the IV section.

II. THEORY AND METHODOLOGY

A. Scintillation detector response

The energy resolution of the scintillation detector is related to Gaussian broadening and can be described by an unbroadening spectrum convoluted with a Gaussian response function. For discrete data, the convolution is given by

$$s(i) = \sum_{k=0}^{i} x(k)h(i-k) = x(i)*h(i) \quad i = 0, 1, \cdots, N+M-1 \tag{1}$$

where $x(k)$ denotes the original input signal, $h(i)$ is the response function, $s(i)$ is the response signal. The same signal length as that of the input signal was obtained by discarding the boundary values.

In real measurements, noise is an inevitable influencing factor in gamma-ray detection systems. Therefore, the scintillation detector response spectrum can be expressed as a matrix equation, as shown in Eq. (2).

$$\boldsymbol{s} = \boldsymbol{H}\boldsymbol{x} + \boldsymbol{n} \tag{2}$$

where $\boldsymbol{s}$ is the scintillation detector response-spectrum vector, $\boldsymbol{x}$ is the gamma-ray energy vector in the detector, $\boldsymbol{n}$ is the noise vector, and $\boldsymbol{H}$ is the Gaussian response matrix.

The Gaussian response matrix determines the extent of energy broadening, which can be written as

$$\boldsymbol{H} = \begin{bmatrix} G_{11} & \cdots & G_{1m} \\ \vdots & \ddots & \vdots \\ G_{m1} & \cdots & G_{mm} \end{bmatrix}_{m\times m} \tag{3}$$

where m denotes the length of the response spectrum vector. The element G_{ij} in the matrix $\boldsymbol{H}$ is expressed as a Gaussian function:

$$G_{ij} = \frac{1}{\sqrt{2\pi}\sigma} \mathrm{e}^{-\frac{(E_i - E_j)^2}{2\sigma^2}} \tag{4}$$

It means that Eq.(4) represents the contribution of a gamma ray with energy E_j to the channel with energy E_i, and σ in Eq.(4) is represented by Eq.(5),

$$\sigma = \frac{1}{2\sqrt{2\ln 2}} FWHM = \frac{1}{2\sqrt{2\ln 2}} (a + b\sqrt{cE^2 + E}) \tag{5}$$

Where $FWHM$ is full width at half maximum, it's a function of a, b, and c; E is the energy of the corresponding channel.

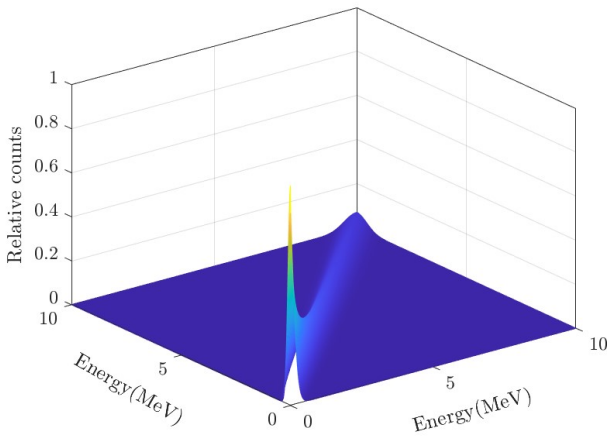

Fig. 1. (Color online) The example of the Gaussian response matrix.

Therefore, the column vector in the matrix $\boldsymbol{H}$ can be regarded as a normalized Gaussian distribution centered on the corresponding diagonal element. Fig. 1 shows an example of a Gaussian response matrix in three-dimensional coordinates with a=0.032, b=0.045, c=0.83.

B. Locally constrained regularization

The key to calibrating the spectral energy resolution is to solve the Gaussian response matrix that matches the response of the gamma-ray measurement system. The solution to the Gaussian response matrix is a typical discrete ill-posed problem, which implies that employing unconstrained least squares cannot yield satisfactory results. Hence, the classical method for solving this type of problem is regularization, which can find a reasonable approximate solution under given constraints. Eq. (6) presents an example of a regularization objective function with a linear approximation constraint using weighted least squares (WLS).

$$F = \operatorname{argmin} \sum_{i=1}^{m} \omega_i (u_i - s_i)^2 + \lambda \sum_{i=2}^{m-1} (\Delta^2 s_i)^2 \tag{6}$$

where s_i and u_i are the ith elements of the calculated and measured vectors, respectively, λ is a regularization parameter that balances both parts of Eq. (6), ω_i is the weight of the ith channel, Δ^2 is the second-order difference operator, which can be expressed as a matrix $\boldsymbol{D}$ shown in Eq. (7). Similarly, quadratic or cubic approximations can be obtained by constructing the corresponding difference matrix [35].

$$\boldsymbol{D} = \begin{bmatrix} 1 & -2 & 1 & 0 & \cdots & 0 & 0 & 0 \\ 0 & 1 & -2 & 1 & \cdots & 0 & 0 & 0 \\ \vdots & \vdots & \vdots & \vdots & \ddots & \vdots & \vdots & \vdots \\ 0 & 0 & 0 & \cdots & 1 & -2 & 1 & 0 \\ 0 & 0 & 0 & \cdots & 0 & 1 & -2 & 1 \end{bmatrix}_{m-2 \times m} \tag{7}$$

Therefore, the objective function can be expressed as a matrix equation, as shown in Eq. (8),

$$\boldsymbol{F}(\boldsymbol{s}) = (\boldsymbol{u} - \boldsymbol{s})^{\mathrm{T}} \boldsymbol{W}_1 (\boldsymbol{u} - \boldsymbol{s}) + \lambda \boldsymbol{s}^{\mathrm{T}} \boldsymbol{D}^{\mathrm{T}} \boldsymbol{D} \boldsymbol{s} \tag{8}$$

where $\boldsymbol{u}$ is the measured vector, $\boldsymbol{s}$ is the calculated vector, $\boldsymbol{W}_1$ is the diagonal weight matrix.

By solving the matrix equation, the optimal solution vector can be obtained when the error between the calculated and measured vectors is minimized.

For spectral resolution calibration, it is difficult to determine an accurate Gaussian response matrix using only the WLS method, particularly in the case of a poor SNR of the gamma spectrum. Fortunately, incident gamma-ray energies are useful prior knowledge in gamma spectral analysis. The energies of neutron-induced or natural gamma rays are related to the inherent properties of nuclei. Based on this premise, the characteristic peaks of gamma rays in the energy spectrum can be used to set additional constraints to determine more accurate energy-resolution parameters.

In the proposed locally constrained regularization method, the objective function can provide additional weights to the peak regions so that the determined energy resolution is more suitable for broadening the characteristic peaks. The new objective function is expressed by Eq. (9):

$$F = \operatorname{argmin} \sum_{i=1}^{m} \omega_{1i} (u_i - s_i)^2 + \lambda \sum_{j=1}^{n} \sum_{i=p_{j1}}^{p_{jk}} [\omega_{2ji} (u_{ji} - s_{ji})]^2 \tag{9}$$

where λ is the regularization parameter, n is the number of selected peak regions, p_{jk} is the number of channels in the jth peak region, w_{1i} is the weight of the ith channel, w_{2ji} is the additional weight of the ith channel in the jth peak region.

The weight of each channel can be designed as a diagonal matrix $\boldsymbol{W}_1$, as expressed in Eq. (10), which is determined by the relative count of the corresponding channel [36].

$$\boldsymbol{W}_1 = \begin{bmatrix} u_1^{-1} & & & & \\ & u_2^{-1} & & & \\ & & \ddots & & \\ & & & u_{m-1}^{-1} & \\ & & & & u_m^{-1} \end{bmatrix}_{m \times m} \tag{10}$$

The additional weights can also be expressed as matrix $\boldsymbol{W}_2$ shown in Eq. (11). The number of columns is equal to the spectral length m, and the number of rows is determined by the number of selected peak regions n.

$$\boldsymbol{W}_2 = \begin{bmatrix} 0 & \cdots & \overbrace{w_{1p_1} \cdots Peak \cdots w_{1p_k}}^{FWHM} & \cdots & \cdots & 0 \\ \vdots & \vdots & \vdots & & \vdots & \vdots \\ 0 & \cdots & \cdots & \underbrace{w_{np_1} \cdots Peak \cdots w_{np_k}}_{FWHM} & \cdots & 0 \end{bmatrix} \tag{11}$$

Only the channels within the $FWHM$ of the selected peak region were assigned additional weights. A nonlinear weighting scheme based on a sigmoid function was designed as shown in Eq. (12):

$$w_{ip} = \operatorname{Sigmoid}(d_{ip}) = \frac{1}{1 + \mathrm{e}^{2(d_{ip} - FWHM/2)/(FWHM/6)}} \tag{12}$$

where w_{ip} is the weight of the pth channel in the ith peak region and d_{ip} is the distance between the pth channel and the peak position of the ith peak region.

In the proposed weighting scheme, the weight of the channel is determined by the distance from the peak position and gradually decreases with an increase in the distance. The channel of the peak position had the maximum weight, and the boundaries of the FWHM had the minimum weight. The weight distributions in the peak regions are shown in Fig. 2(a). Channels within the FWHM of the spectral peak were assigned additional weights using this weighting scheme, as shown in Fig. 2(b)). Similarly, the new objective function of the locally constrained regularization can be expressed as a matrix equation:

$$\boldsymbol{F}(\boldsymbol{s}) = (\boldsymbol{u} - \boldsymbol{s})^{\mathrm{T}} \boldsymbol{W}_1 (\boldsymbol{u} - \boldsymbol{s}) + \lambda (\boldsymbol{u} - \boldsymbol{s})^{\mathrm{T}} \boldsymbol{W}_2^{\mathrm{T}} \boldsymbol{W}_2 (\boldsymbol{u} - \boldsymbol{s}) \tag{13}$$

Finally, the objective function is converted into a function of a Gaussian response matrix.

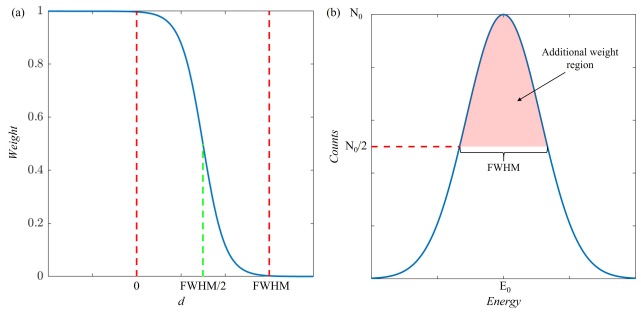

Fig. 2. (Color online) (a)The weight distribution of the peak region; (b)The additional weight region of the peak region

$$\boldsymbol{F}(\boldsymbol{H}) = (\boldsymbol{u}-\boldsymbol{H}\boldsymbol{x})^{\mathrm{T}}\boldsymbol{W}_1(\boldsymbol{u}-\boldsymbol{H}\boldsymbol{x})+\lambda(\boldsymbol{u}-\boldsymbol{H}\boldsymbol{x})^{\mathrm{T}}\boldsymbol{W}_2^{\mathrm{T}}\boldsymbol{W}_2(\boldsymbol{u}-\boldsymbol{H}\boldsymbol{x}) \tag{14}$$

C. Energy resolution calibration

A strong correlation exists between the elements in the Gaussian response matrix, which is determined by a broadening mechanism. Thus, the objective function can be regarded as a function of resolution calibration parameters a, b, and c. Calibrating the energy resolution can be considered a high-dimensional constrained optimization problem, which can be expressed as Eq.(15), where N is the number of measured spectra:

$$\min \sum_{i=1}^{N} f_i(a,b,c) \quad s.t. a,b,c \geq 0 \tag{15}$$

The swarm intelligence optimization algorithm is an iterative method that updates feasible solutions based on their fitness. It has the advantage that it does not depend on the initial guess and does not require a derivative of the objective function. Therefore, we adopt the particle swarm optimization (PSO) to achieve the global optimal solution of the objective function.

PSO is a classical optimization algorithm inspired by bird predation behaviors. PSO initializes a group of particles as potential solutions, and the fitness of the solution is determined by the objective function. In the kth iteration, the ith particle updates its velocity $\boldsymbol{V}_i^k$ and position $\boldsymbol{X}_i^k$ by tracking the individual optimum position $\boldsymbol{P}_i^k$ and global optimum position $\boldsymbol{P}_g^k$ to search for the optimal solution, as shown in Eq. (16) and Eq. (17) [37].

$$\boldsymbol{V}_i^{k+1} = \omega \boldsymbol{V}_i^k + c_1 r_1(\boldsymbol{P}_i^k - \boldsymbol{X}_i^k) + c_2 r_2(\boldsymbol{P}_g^k - \boldsymbol{X}_i^k) \tag{16}$$

$$\boldsymbol{X}_i^{k+1} = \boldsymbol{X}_i^k + \boldsymbol{V}_i^{k+1} \tag{17}$$

where ω is the inertia weight, c_1 and c_2 are the acceleration factors, r_1 and r_2 are random numbers distributed between[0, 1].

Another key parameter in the objective function is the incident gamma ray energy vector $\boldsymbol{x}$. As mentioned above, Monte Carlo simulation is a useful method for obtaining the response of a gamma-ray measurement system, which can solve neutron, photon, electron, or coupled neutron/photon/electron transport problems in a three-dimensional complex geometry. The gamma-ray energy distribution in the scintillation detector can be effectively obtained by establishing a simulation model consistent with the actual measurement system. Then, utilizing the simulated gamma ray energy distribution, the error between the measured and calibrated spectra was computed based on the established objective function under the preset constraints. Normalization is required in the calculation to ensure that the measured and calibrated spectra are of the same order of magnitude. This error can be used as a fitness evaluation criterion to update the particle swarm using the PSO algorithm. A flowchart of the energy-resolution calibration using the locally constrained regularization method is shown in Fig. 3.

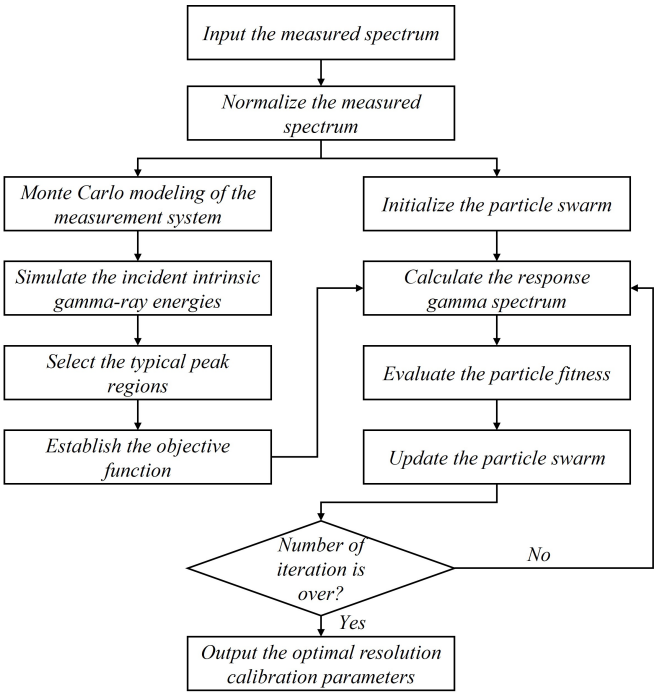

Fig. 3. (Color online) The flowchart of energy resolution calibration by locally constrained regularization method

III. EXPERIMENTS AND DISCUSSIONS

A. Experiments on simulated spectra

To verify the performance of the proposed locally constrained regularization method, a Monte Carlo simulation model was constructed based on an actual NaI detector structure, as shown in Fig. 4. The diameter and length of the NaI scintillation crystals were 3.18 cm, and 10.16 cm. The NaI

crystal was coated with a MgO reflecting layer with a thickness of 0.05 cm. The outermost layer of the detector was an aluminum shell with a thickness of 0.1cm. One end of the detector was a light guide made of SiO_2, which is 0.2 cm thick. A gamma source that can emit gamma rays with a specified energy distribution was set in front of the detector. As neutrons are transported in a medium, they gradually thermalize because they collide numerous times with the nuclei of the medium. Thermal neutrons are then captured by the target nucleus to release gamma photons. The energies of the neutron-induced gamma rays determined by the type of the elements can be regarded as the elemental "fingerprint." In the simulation experiments, the thermal neutron-captured gamma rays of four common elements, H, Si, Al, and Ca, were used as the incident gamma-ray energy distributions [38], as shown in Fig. 5. The gamma source of the simulation model emitted gamma rays that followed the above four distributions, and the simulated gamma rays with energies ranging from 0.088 MeV to 10 MeV were recorded in 1024 channels as the experimental test set. Random noise was added to each simulated spectrum to illustrate the applicability of the proposed method.

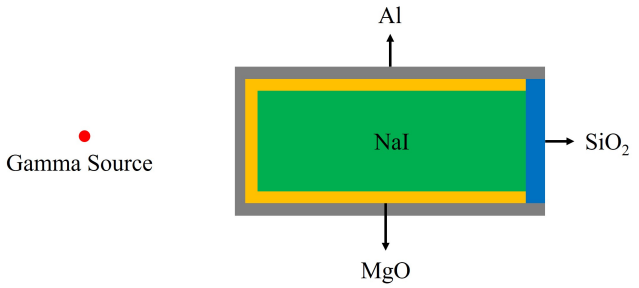

Fig. 4. (Color online) The model for the simulated spectra

For the regularization method, the regularization parameter is the key factor affecting performance. The main function of the regularization parameter is to balance the importance of the sum of the weighted squares of the errors and constraints. Therefore, mathematical experiments were conducted to determine the most appropriate regularization parameters. In the experiments, the weight of each channel in the matrix $\boldsymbol{W}_1$ was determined by the corresponding intensity expressed in Eq. (10), and part of the characteristic gamma-ray energies of the four elemental energy distributions whose intensities are larger than 10% are selected to construct the regularization weight matrix $\boldsymbol{W}_2$. Regularization parameters 10, 20, 30, 50, 70, and 100 were used to establish the objective function, and the PSO algorithm was adopted to search for the optimal resolution calibration parameters with different regularization parameters. The average RMSEs of the spectra of the H, Si, Al, and Ca elements between the calibrated and simulated spectra with different regularization parameters are shown in Fig. 6. It can be found that the calibrated spectra have the minimum RMSE when the regularization parameter is about 30. These conclusions can guide the application of the proposed method.

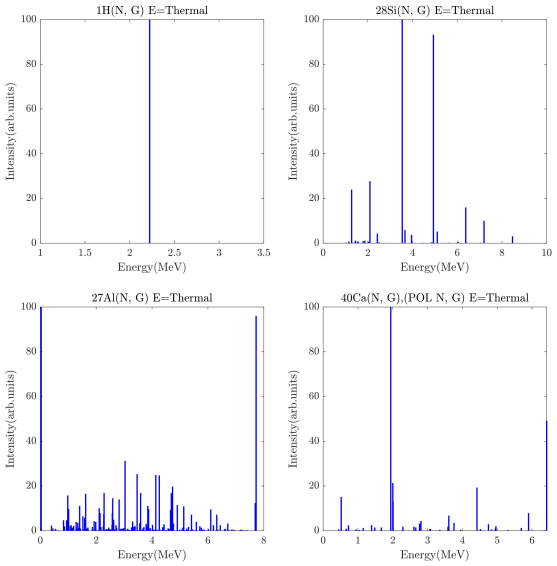

Fig. 5. (Color online) The capture gamma-ray energy distributions of H, Si, Al, and Ca elements

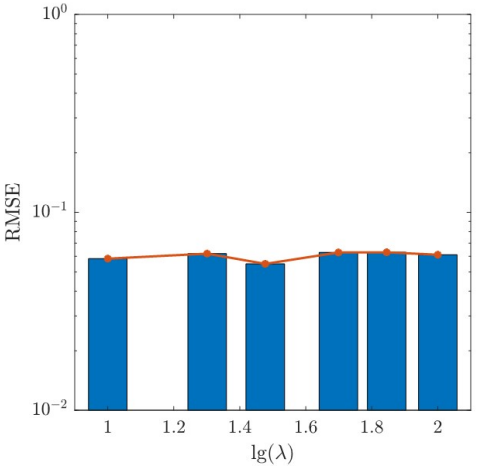

Fig. 6. (Color online) The average RMSEs between the original spectra and the calibrated spectra with different regularization parameters

A comparison between the simulated and calibrated spectra is shown in Fig. 7. Even for spectra with noise, the resolution calibration parameters determined by the proposed locally constrained regularization method still have a high consistency with the simulated spectra. The correlation coefficients between all the simulated spectra and the corresponding calibrated spectra were greater than 0.99, which indicates the applicability of the proposed method.

The performances of the locally constrained regularization and traditional weighted least squares were also compared to illustrate their applicability. Resolution calibration results for the Al spectra obtained using the two methods are shown in Fig. 8. This is shown in Fig. 8(a), the resolution calibration parameters determined using the locally constrained

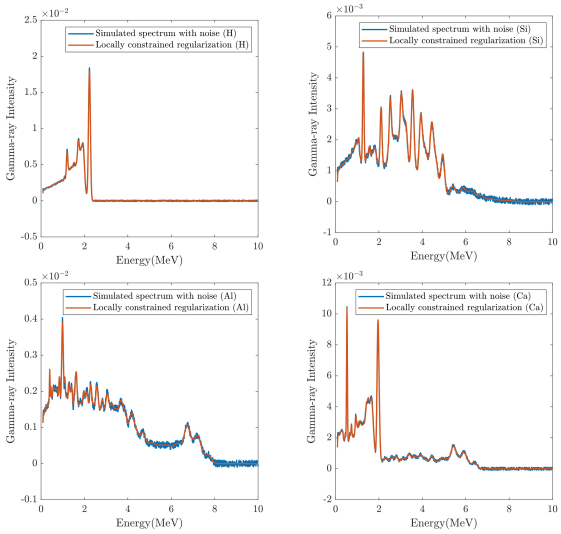

Fig. 7. (Color online) The resolution extraction results of the locally constrained regularization method for different elemental spectra

regularization method cause each characteristic peak of the calibration spectrum to match the corresponding characteristic peak of the simulation spectrum. In contrast, although the spectrum calibrated by the weighted least squares is well consistent with the simulated spectrum in the energy range of 3.5 MeV-6 MeV, the resolution error of the characteristic peaks in the energy range of 0.5 MeV-3.5 MeV and 6 MeV-8 MeV is relatively large because of the lack of sufficient constraints, as shown in Fig. 8(b)).

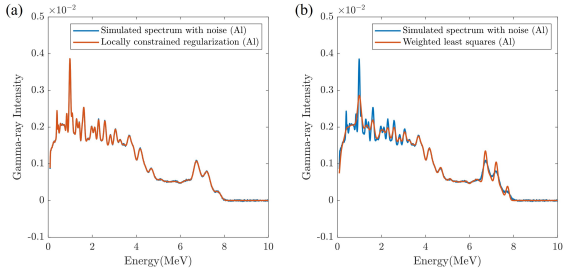

Fig. 8. (Color online) The resolution calibration results of the Al spectrum using the locally constrained regularization method and weight least squares

The optimal resolution calibration parameters of the two methods were determined by the PSO algorithm using 1000 iterations. The iterative curves of the locally constrained regularization method and the weighted least-squares method are shown in Fig. 9. We found that the RMSEs of the two methods gradually decreased with the iterations, indicating that the fitness of the objective function was enhanced. Although the iterative curve of the weighted least squares method has a faster convergence rate during the iteration, the final RMSE is higher than that of the proposed method, which means that the optimization is trapped in a locally optimal solution.

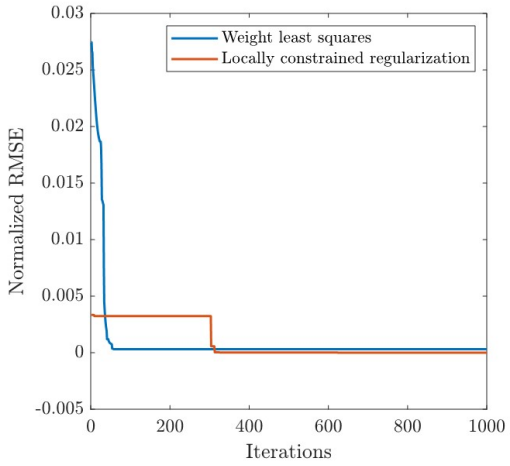

Fig. 9. (Color online) Comparison of the iterative curves of the locally constrained regularization method and weight least squares

B. Experiments on measured spectra

Pulsed neutron logging is a powerful method for detecting and analyze reservoir elemental compositions and has been widely used in oilfield exploration and development. The logging instrument was a typical neutron-induced gamma-ray measurement system. It usually uses a D-T neutron source to excite the nuclei of formation elements to release gamma rays and uses scintillation detectors to obtain the corresponding gamma energy spectra. Therefore, test pit experiments for pulsed neutron logging were performed to verify the performance of the proposed locally constrained regularization method for spectral resolution calibration. The experimental pulsed neutron logging instrument was set in different artificial pits with known compositions and geometric structures. As shown in Fig. 10 (a), several test pits are located at the experimental site. The configurations of the pure rock and simple substance test pits are shown in Fig. 10 (b)). The depth of these test pits was 6050 mm and they were divided into multiple intervals. The intervals are filled with different materials, including aluminum (Al), magnesium (Mg), iron (Fe), titanium (Ti), graphite (C), limestone (LS), and granite (GS). The instrument was inserted into a borehole with a diameter of 200 mm, which was filled with fresh water, to measure neutron-induced gamma-rays. In the experiments, four test pits were selected as the measurement objects, three of which were pure rock or simple substance test pits (LS, Al, and C), and the fourth was a water tank. As described in the Methodology section, a Monte Carlo simulation model was constructed based on the actual experimental instrument structure and test pit configurations to simulate the energy deposition distribution in the scintillation crystal, as shown in Fig. 11. The diameter and length of the instrument were SI41mmand 2358 mm. The D-T neutron source consisted of an accelerating system and a neutron-producing target. The instrument has three scintillation detectors with different source-detector spacings (29 cm, 59 cm and 91 cm), and

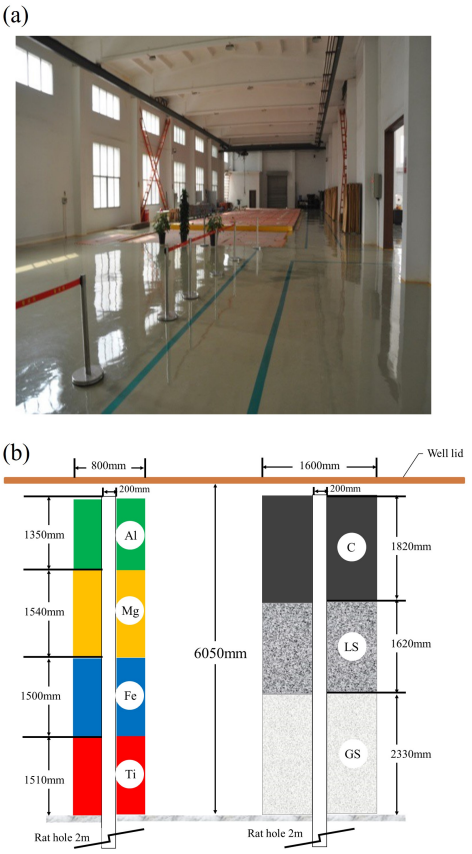

Fig. 10. (Color online) The test pit experimental site (a) and the configurations of pure rock or substance test pits (b)

there is a tungsten shield between the source and the nearby detector. The far and near detectors use $LaBr_3$ crystals with crystal sizes of $27.5\,\mathrm{mm}\times152\,\mathrm{mm}$ and $27.5\,\mathrm{mm}\times38\,\mathrm{mm}$ (diameter$\times$length), respectively. The extra detector adopts a NaI crystal of size $27\,\mathrm{mm}\times152\,\mathrm{mm}$. The extra detector has the maximum spacing; therefore, it is mainly used to collect natural gamma-rays rather than neutron-induced gamma-rays. In the experiments, considering the influence of radioactive statistical fluctuations on gamma-ray spectral measurements, the energy spectrum collected by the near detector was selected to test the proposed method.

Based on the mechanism of nuclear reactions between fast neutrons and nuclei, two types of interactions can produce secondary gamma-rays: inelastic collisions and capture reactions. The experimental instrument utilized a special measurement sequence to measure and capture inelastic secondary gamma rays. As shown in Fig. 12, the D-T neutron source of the instrument periodically emits neutrons with energies of $14\,\mathrm{MeV}$. The complete measurement period of 20ms consists of 200 subperiods of $100\,\mu\mathrm{s}$, where the neutron source emitted neutrons during the first $40\,\mu\mathrm{s}$ of each subperiod, whereas the neutron source did not work for the next $60\,\mu\mathrm{s}$. In the measurement, the scintillation detector recorded the gamma ray energy spectra during the G2 and G3 time gates and then accumulated the spectra of all sub-periods

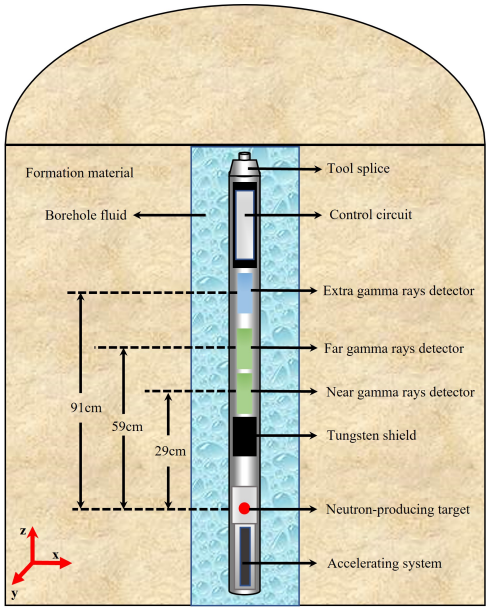

Fig. 11. (Color online) The test pit experimental Monte Carlo model

to obtain the final energy spectra. In general, inelastic collision and capture reactions occur during the neutron burst time (G2), whereas only the capture reaction can occur during the G3 time gate, when the neutron source stops working. Therefore, the spectrum obtained in time gate G2 is called the total spectrum, which contains inelastic secondary gamma-rays and captures secondary gamma-rays, whereas the spectrum obtained in time gate G3 is called the capture spectrum, which only contains captured secondary gamma-rays. The proposed

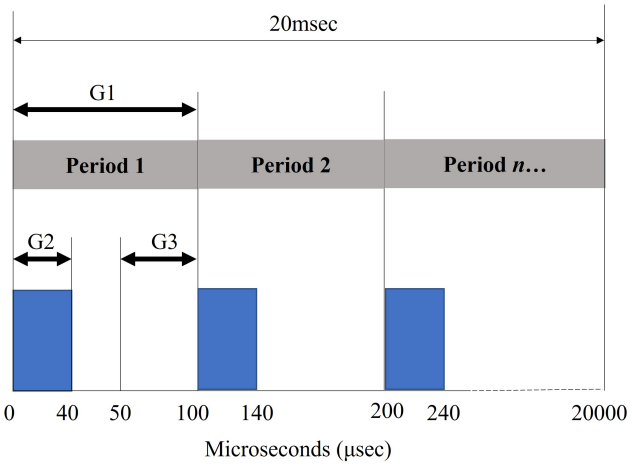

Fig. 12. (Color online) The measurement sequence of the experimental instrument

locally constrained regularization method was used to calibrate the energy resolution using two types of spectra. All the total and capture spectra measured in the four test pits were used to establish the objective function. After optimization, the optimal resolution calibration parameters were a= 0.0479,

b= 0.0146, and c= 8.3718. Obviously, the determined resolution calibration parameters apply to all the spectra measured by the instrument.

The calibration results for the entire spectrum are shown in Fig. 13. It can be seen that each total spectrum has an apparent characteristic peak with an energy of 2.23 MeV, which is produced by the capture reaction of hydrogen in the borehole fluid. In addition, some characteristic peaks of other elements were observed in the total spectra, such as the inelastic characteristic peaks of oxygen (6.13 MeV) and carbon (4.43 MeV) in the water tank and graphite test pit. All the characteristic peaks, including the corresponding escape peaks, can be used to set additional constraints as useful prior knowledge.

The selected characteristic peaks of each total spectrum, RMSE, and correlation coefficient (R-Square) between the normalized experimental spectrum and normalized calibrated spectrum are shown in Table 1. In the experiment, distinct peaks were selected for each spectrum to set the constraint conditions. We found that there were good correlations between the experimental and calibrated spectra from the comparison results. All correlation coefficients were greater than 0.99, and the average RMSE was only 4.22×10^{-4} after resolution calibration using the locally constrained regularization method.

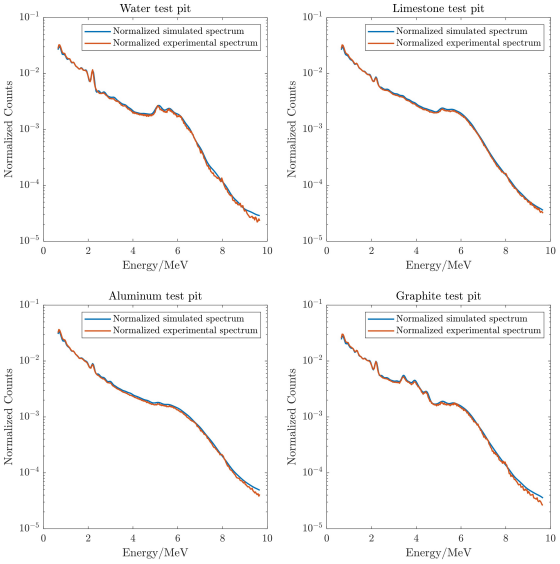

Fig. 13. (Color online) The comparison of the experimental spectra and the calibrated spectra of different test pits (total spectrum)

Comparisons of the normalized experimental capture spectra with the normalized calibrated capture spectra are shown in Fig. 14, and the capture spectral calibration results for the four test pits are listed in Table 2. The characteristic peak of hydrogen was also observed in all four measured spectra. In addition, the characteristic peaks of calcium (6.42 MeV) and aluminum (3.03 MeV and 4.69 MeV) were selected to set constraints for the spectra of the corresponding test pits. From the comparison results, it can be observed that the correlations between the calibrated and measured spectra are sufficient. All correlation coefficients were greater than 0.99, and the average RMSE was 4.03e-4. The calibration results of the capture spectra also proved the performance of the locally constrained regularization method in spectral-resolution calibration.

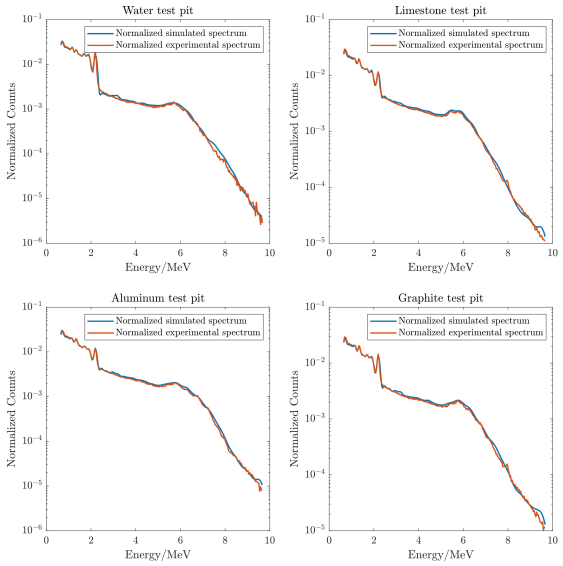

Fig. 14. (Color online) The comparison of the experimental spectra and the calibrated spectra of different test pits (capture spectrum)

IV. CONCLUSIONS

This study proposes a locally constrained regularization method to calibrate gamma-ray spectral energy resolution. The objective function of the proposed method was designed based on the convolution of the incident gamma-ray energy distribution and the detector response function. The incident gamma-ray energies, which are determined by the nuclear properties, are used as a type of prior knowledge to set additional constraints on the objective function. A special nonlinear weighted scheme is introduced to provide additional weights to the channels within the FWHM of the spectral peak to ensure that the characteristic peak broadening can match the actual resolution. Because of the spectral broadening mechanism, the elements in the response matrix exhibit a strong correlation. Hence, the optimal resolution calibration parameters were determined by combining an intelligent algorithm and Monte Carlo simulation. The most appropriate regularization parameters were determined through mathematical experiments. The results show that when the value is 30, the regularization parameter can balance the importance between the sum of the weighted squares of the errors and the constraints. The processing results of the proposed method were compared with those of the weighted least squares method using simulated spectra, which proved the calibrated resolution accuracy. The measured spectral processing results in the test pits also showed that the calibrated spectra were consistent with the measured spectra obtained

Table 1. The comparison of the normalized experimental spectrum with the normalized calibrated spectrum of the total spectra

Test pit	Characteristic peaks (MeV)	RMSE	R-Square
Water	2.23, 5.11, 6.13	4.16×10^{-4}	0.9954
Limestone	2.23, 5.40, 6.42	4.18×10^{-4}	0.9947
Aluminum	2.23, 3.03, 4.69	4.57×10^{-4}	0.9947
Graphite	2.23, 3.41, 4.43	3.98×10^{-4}	0.9950

Table 2. The comparison of the normalized experimental spectrum with the normalized calibrated spectrum of the capture spectra

Test pit	Characteristic peaks (MeV)	RMSE	R-Square
Water	2.23	5.18×10^{-4}	0.9950
Limestone	2.23, 5.40, 6.42	3.53×10^{-4}	0.9966
Aluminum	2.23, 3.03, 4.69	3.66×10^{-4}	0.9965
Graphite	2.23	3.76×10^{-4}	0.9963

using the resolution calibration parameters determined using the proposed method.

CONFLICTS OF INTEREST

The authors declare no conflict of interest. We declare no commercial or associative interests that represent a conflict of interest in connection with the submitted work.

[1] J. Wang, Y. Zhang, D. Liu et al., Automated spectra analysis of in situ radioactivity measurements in the marine environment using NaI(Tl) detector. Appl. Radiat. Isot. **141**, 88–94 (2018). doi:10.1016/j.apradiso.2018.08.026

[2] X. Xu, J. Lu, Y. Chang et al., Measurement of talc in flour by the prompt-gamma ray neutron activation analysis method. Appl. Radiat. Isot. **178**, 109932 (2021). doi:10.1016/j.apradiso.2021.109932

[3] Q. Zhang, Y. Ge, Y. Li, Source-less density measurement using an adaptive neutron-induced gamma correction method. Nucl. Sci. Tech. **8**, 115–130 (2023). doi:10.1007/s41365-023-01274-4

[4] Y. Ge, Q. Zhang, A novel quantitative measurement method for formation element via iterative support vector regression. Geoenergy Sci. Eng. **230**, 212230 (2023). doi:10.1016/j.geoen.2023.212230

[5] A. Mostafa, H. Zakaly, S. Al-Ghamdi et al., PbO–Sb_2O_3–B_2O_3–CuO glassy system: evaluation of optical, gamma and neutron shielding properties. Mater. Chem. Phys. **258**, 123937 (2021). doi:10.1016/j.matchemphys.2020.123937

[6] H. Saudi, H. Tekin, H. Zakaly et al., The impact of samarium (III) oxide on structural, optical and radiation shielding properties of thallium-borate glasses: experimental and numerical investigation. Opt. Mater. **114**, 110948 (2021). doi:10.1016/j.optmat.2021.110948

[7] M. Rashad, H. Saudi, H. Zakaly et al., Control optical characterizations of Ta^{+5}–doped B_2O_3–Si_2O–CaO–BaO glasses by irradiation dose. Opt. Mater. **112**, 110613 (2021). doi:10.1016/j.optmat.2020.110613

[8] H. Zakaly, H. Saudi, H. Tekin et al., Glass fabrication using ceramic and porcelain recycled waste and lithium niobate: physical, structural, optical and nuclear radiation attenuation properties. J. Mater. Res. Technol. **15**, 4074–4085 (2021). doi:10.1016/j.jmrt.2021.09.138

[9] C. Celiktas, E. Ermis, M. Bayburt, Energy resolution improvement of NaI(Tl) scintillation detectors by means of a timing discrimination method. J. Radioanal. Nucl. Chem. **293**, 377–382 (2012). doi:10.1007/s10967-012-1678-1

[10] C. Celiktas, E. Ermis, E. Pilicer, Note on the comparison of experimental and simulated gamma energy spectra for NaI with ^{137}Cs, ^{60}Co, and ^{241}Am. Ann. Nucl. Energy **73**, 355–360 (2014). doi:10.1016/j.anucene.2014.06.044

[11] S. Zhang, C. Liu, X. Yang, Study of unfolded gamma spectra by using EJ309 liquid scintillator detector. Nucl. Instrum. Methods A **1006**, 165407 (2021). doi:10.1016/j.nima.2021.165407

[12] Y. Eltaher, S. Ma. Carbon/Oxygen spectral data processing, its affiliation to scintillation detector selectivity & their impact on reservoir saturation monitoring, lessons learnt and recommended workflow. In: SPE Reservoir Characterisation and Simulation Conference and Exhibition (2023). doi:10.2118/212613-MS

[13] J. Brechtl, X., Xie, R. Feng et al. Serrated flow in NaI:Tl scintillator crystals. J. Mater. Sci. Technol. **153**, 120–127 (2023). doi:10.1016/j.jmst.2022.12.047

[14] J. Maebe, S. Vandenberghe. Effect of detector geometry and surface finish on Cerenkov based time estimation in monolithic BGO detectors. Phys. Med. Biol. **68**, 1–11 (2023). doi:10.1088/1361-6560/acabfd

[15] H. Bi, Y. Zhang, B. Wu et al., Study on reconstruction and analytical method of seawater radioactive gamma spectrum. Appl. Radiat. Isot. **198**, 110853 (2023). doi:10.1016/j.apradiso.2023.110853

[16] J. He, Y. Yang, J. Qu et al., An inversion decomposition method for better energy resolution of NaI (Tl) scintillation detectors based on a Gaussian response matrix. Nucl. Sci. Tech. **27**, 58 (2016). doi:10.1007/s41365-016-0062-1

[17] K. Nelson, T. Gosnell, David Knapp, The effect of energy resolution on the extraction of information content from gamma-ray spectra. Nucl. Instrum. Methods A **659**, 207–214 (2011). doi:10.1016/j.nima.2011.06.057

[18] L. Amri, A. Chetaine, H. Amsil, New open-source software for gamma-ray spectra analysis. Appl. Radiat. Isot. **185**, 110227 (2023). doi:10.1016/j.apradiso.2022.110227

[19] I. Espagnon, P. Allinei, A. Simon et al. MAGIX, a new software for the analysis of complex gamma spectra. Appl. Radiat. Isot. **191**, 110505 (2023). doi:10.1016/j.apradiso.2022.110505

[20] R. Shi, X. Tuo, H. Li et al., Unfolding analysis of LaBr3: Ce gamma spectrum with a detector response matrix constructing algorithm based on energy resolution calibration. Nucl. Sci. Tech. **29**, 1 (2018). doi:10.1007/s41365-017-0340-6

[21] J. Li, W. Xiao, X. Ai et al., Nonnegative constraint quadratic program technique to enhance the resolution of γ spectra. Nucl. Instrum. Methods A **887**, 169–173 (2018). doi:10.1016/j.nima.2018.01.022

[22] M. El_Tokhy, Rapid and robust radioisotopes identification algorithms of X-Ray and gamma spectra. Measurement **168**, 108456 (2021). doi:10.1016/j.measurement.2020.108456

[23] J. He, Q. Wu, J. Chen et al., An inversion decomposition test based on Monte Carlo response matrix on the γ-ray spectra from NaI (Tl) scintillation detector. Nucl. Sci. Tech. **27**, 101 (2016). doi:10.1007/s41365-016-0104-8

[24] H. Wei, N. Wang, Efficiency calibration for a NaI scintillation detector based on Monte-Carlo process and preliminary measurements of bremsstrahlung. Acta Phys. Sin. **63**, 180702 (2014). doi:10.7498/aps.63.180702

[25] H. Zhu, G. Wang, C. Yang et al., Overlapped peaks resolution for linear sweep polarography using Gaussian-like distribution. Trans. Nonferrous Met. Soc. **23**, 2181–2186 (2013). doi:10.1016/S1003-6326(13)62715-6

[26] M. Morháč, J. Kliman, M. Jandel et al., Study of fitting algorithms applied to simultaneous analysis of large numbers of peaks in γ-ray spectra. Appl. Spectrosc. **57**, 753–760 (2003). doi:10.1366/000370203322102825

[27] M. Kwak, B. Lkhagvasuren, X. Sun, An efficient method for fitting Gaussian functions. Iran. J. Sci. Technol. **45**, 1043–1056 (2021). doi:10.1007/s40995-021-01079-3

[28] H. Guo, A simple algorithm for fitting a Gaussian function. IEEE Signal Proc. Mag. **28**, 134–137 (2011). doi:10.1109/MSP.2011.941846

[29] C. Ryan, E. Clayton, W. Griffin et al., SNIP, a statistics-sensitive background treatment for the quantitative analysis of PIXE spectra in geoscience applications. Nucl. Instrum. Methods Phys. Res., Sect. B **34**, 396–402 (1988). doi:10.1016/0168-583X(88)90063-8

[30] S. Baek, A. Park, Y. Ahn et al. Baseline correction using asymmetrically reweighted penalized least squares smoothing. Analyst. **140**, 250 (2015). doi:10.1039/c4an01061b

[31] G. Yang, J. Dai, X. Liu et al., Multiple constrained reweighted penalized least squares for spectral baseline correction. Appl. Spectrosc. **74**, 1443–1451 (2020). doi:10.1177/0003702819885002

[32] H. Sahiner, X. Liu, Gamma spectral analysis by artificial neural network coupled with Monte Carlo simulations. Nucl. Instrum. Methods A **953**, 163062 (2020). doi:10.1016/j.nima.2019.163062

[33] N. Elsheikh, Characterization of (^{252}Cf-ZrH$_2$) Monte Carlo model for detection of nitrogen and chlorine by thermal neutron-capture PGNAA. Radiat. Phys. Chem. **188**, 109591 (2021). doi:10.1016/j.radphyschem.2021.109591

[34] W. Wang, J. Liang, Y. Ge et al., A method for neutron-induced gamma spectra decomposition analysis based on Geant4 simulation. Nucl. Sci. Tech. **33**, 154 (2022). doi:10.1007/s41365-022-01144-5

[35] M. Morhac, V. Matousek, Complete positive deconvolution of spectrometric data. Digit. Signal Process. **19**, 372 (2009). doi:10.1016/j.dsp.2008.06.002

[36] N. Heckert, J. Filliben, C. Croarkin et al., Handbook 151: NIST/SEMATECH e-handbook of statistical methods. (2002). doi:10.18434/M32189

[37] G. Yang, X. Liu, J. Dai et al., Injection profile surveillance using impulse oxygen activation logging based on optimization theory. J. Pet. Sci. Eng. **196**, 107701 (2021). doi:10.1016/j.petrol.2020.107701

[38] M. Chadwick, P. Oblozinsky, M. Herman et al. ENDF/B-VII. 0: next generation evaluated nuclear data library for nuclear science and technology. Nucl. Data Sheets **107**, 2931–3060 (2006). doi:10.1016/j.nds.2006.11.001